THE AMERICAN MINERALOGIST, VOL. 56, JANUARY–FEBRUARY, 1971

POSITION OF ISOCHROMES IN INTERFERENCE FIGURES

BARCLAY KAMB, *Division of Geological Sciences,*[1] *California Institute of Technology, Pasadena, California 91109.*

ABSTRACT

Isochromes positions in two different types of uniaxial interference figure are explained theoretically. For figures of one type (Fisher's "images") Mallard's Rule is valid.

A useful test of the theory of color distribution in interference figures (Kamb, 1970) is provided by some measurements made by Fisher (1960) on uniaxial optic axis figures of two types: (1) figures obtained with a high-power microscope objective, and enlarged to an image about 6 cm in diameter by means of an auxiliary lens; (2) figures obtained by direct projection from essentially a point source of light, through the crystal (between crossed polaroids), and onto a screen. Figures of type 1, which Fisher calls "images," can be regarded as the standard type of figure seen in the polarizing microscope, the Bertrand lens taking the place of the auxiliary lens (actually a low-power objective) used by Fisher. Figures of type 2, called "pictures" by Fisher, are convenient for large-scale demonstrations of interference phenomena, particularly with sheets of muscovite. Fisher measured the radii of centered uniaxial isochromatic curves in the two types of figures, and found large discrepancies between the two for the curves of higher order. In the present note I wish to show how Fisher's measurements can be explained. In addition to providing a test of the theory, the measurements also serve to confirm the validity of Mallard's Rule, to a good approximation.

Figures 1 and 2 show the optical arrangement used in obtaining the two types of figure. If for type 1 figures we idealize the microscope objective lens by a simple hemisphere O, then we obtain an optical geometry that leads to Mallard's Rule for the relation between the initial ray inclination θ and the radial distance r_1 in Figure 1:

$$r_1 = l_1 \sin \theta \tag{1}$$

l_1 is the effective Mallard's constant for the objective lens, and is given, from Figure 1, by $l_1 = Rl''/l'$. Note that (1) follows from the geometry of Figure 1 only in the approximation that $l' \gg R$, so that P' lies essentially a constant distance l' from lens L, and r_1 is proportional to r'. The actual objective, being a compound lens system of rather complex design, does not necessarily admit of the idealization in Figure 1, and does not neces-

[1] Contribution No. 1898.

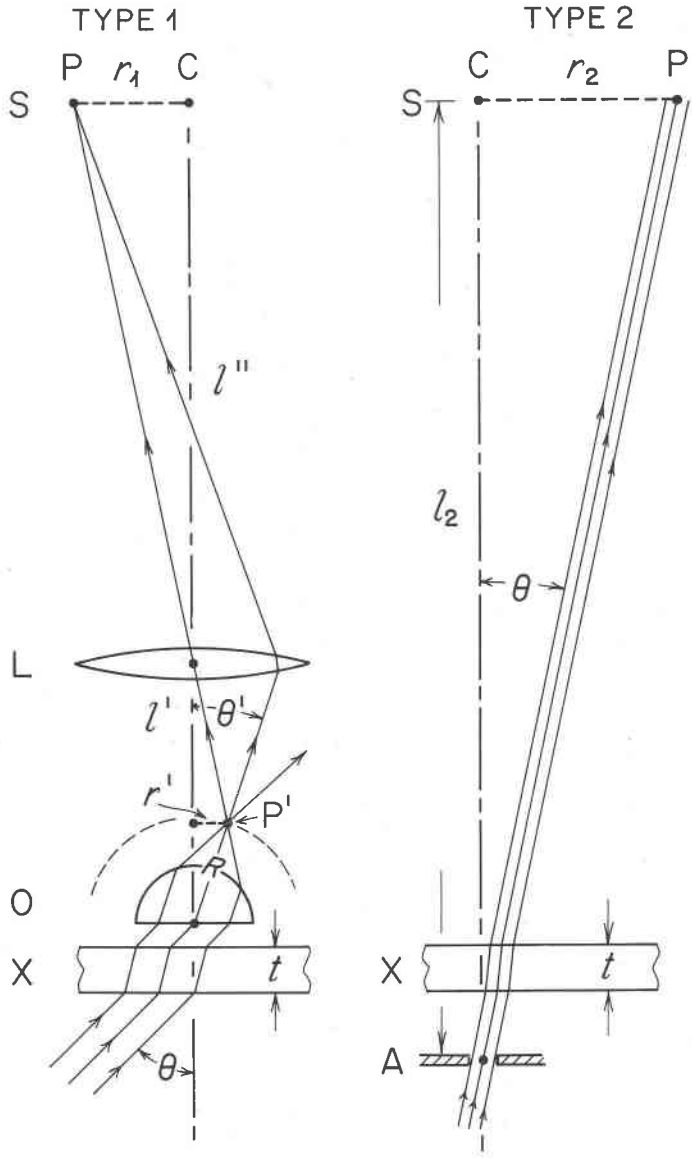

FIG. 1 (*left*) and FIG. 2 (*right*). Optical geometry in interference figures of type 1 (left) and type 2 (right). Light rays (thin lines) that enter the crystal plate X at an angle θ to its normal arrive ultimately at point P on screens, where the interference figure is observed. P lies a distance r_1 or r_2 from the centerpoint C. In type 1 figures, C is is defined by the optical axis of the lens system, and in type 2 by the projection of aperture A along the

sarily therefore satisfy Mallard's Rule, equation (1). However, we will here use (1) provisionally, and show that for the objective lens used by Fisher (1) works to a good approximation.

For type 2 figures (Fig. 2), the optical geometry is particularly simple. Rays which entered the crystal plate at an angle θ with respect to its normal are projected to a point P at a distance r_2 from the center C, given by

$$r_2 = l_2 \tan \theta \tag{2}$$

(2) is valid if $t \ll l_2$ (see Fig. 2).

In Table 1 (columns 2 and 5) are listed the sequences of values $r_1(m)$ and $r_2(m)$ measured by Fisher (1960, Table 1) for the dark curves of successive orders m in centered optic axis figures from an essentially uniaxial piece of muscovite, under Hg-vapor light. The measured radii r_1 and r_2 were scaled by Fisher so that $r_1(1) = r_2(1)$; the projection distance l_2 and the effective Mallard's constant l_1 were not given. If equations (1) and (2) hold for the r_1 and r_2 values, then they should satisfy

$$\left(\frac{r_1(m)}{r_2(m)}\right)^2 = \left(\frac{l_1}{l_2}\right)^2 - \left(\frac{l_0}{l_2}\right)^2 \left(\frac{r_1(m)}{l_0}\right)^2 \tag{3}$$

obtained from (1) and (2) by eliminating θ. In (3), l_0 is an arbitrary scaling distance introduced for convenience. Fig. 3 shows a plot of $(r_1/r_2)^2$ against $(r_1/l_0)^2$ (with $l_0 = 20.0$ mm). It shows that the measured values in Table 1 satisfy (3) to a fairly good approximation. The small systematic departure of the points from a straight line in Fig. 3 probably reflects some inaccuracy in equation (1), meaning that the microscope objective does not satisfy Mallard's Rule exactly. From the intercept of the straight line fitted to the points in Fig. 3 we obtain $l_1/l_2 = 1.048$, and from the slope, $l_2/l_0 = 3.87$. Hence we deduce $l_1 = 81.1$ mm and $l_2 = 77.4$ mm, distances which are reasonable in relation to the experiments described by Fisher (1960).

---

normal to the crystal plate. The objective lens O used in forming type 1 figures is here idealized as a hemisphere of focal length R; from the focal hemisphere (dashed) the figure is imaged by Bertrand lens L onto screen S. In type 2 figures, aperture A serves to define a small, nearly point source of light at distance l_2 from screen S; sharpness of the interference effect seen at P depends on having an adequately small aperture A, so that all of the rays arriving near P travelled through the crystal plate at nearly the same angle, as shown. Polarizer and analyzer are omitted from the figures, as are details of refraction of the light rays within the anisotropic crystal plate.

TABLE 1. ISOCHROME RADII FOR CENTERED UNIAXIAL FIGURES

1	2	3	4	5	6
	Type-1 Figure			Type-2 Figure	
Order m	Obs. r_1	Calc. r_1	"$\sqrt{m}$" r	Obs. r_2	Calc. r_2
1	20.0	20.3	20.0	20.0	20.1
2	28.6	28.6	28.4	29.1	29.1
3	35.0	34.8	34.7	36.9	36.8
4	40.0	39.9	40.0	43.7	43.8
5	44.2	44.3	44.8	50.4	50.4
6	47.9	48.2	49.0	57.1	57.1
7	51.3	51.8	53.0	63.6	64.0
8	54.7	55.0	56.6	70.5	71.2
9	57.4	58.0	60.0	—	—

Explanation

Col. 2. Radii measured by Fisher (1960, Table 1, "Image").
3. Calculated from eqns. (1) and (6).
4. Calculated by Fisher (1960, Table 1, "$\sqrt{m}$ rule").
5. Radii measured by Fisher (1960, Table 1, "Picture").
6. Calculated from eqns. (2) and (6).

From the theory (Kamb, 1970)[1] we obtain the following relation between ray inclination θ (see Figs. 1 and 2) and path difference Δs for a uniaxial crystal plate of thickness t, with optic axis normal to the plate:

$$\Delta s = t\omega\left(\sqrt{1-\frac{\sin^2\theta}{\epsilon^2}}-\sqrt{1-\frac{\sin^2\theta}{\omega^2}}\right) \tag{4}$$

(ϵ and ω are the extraordinary and ordinary refractive indices.) The angles $\theta(m)$ for successive orders of isochromatic curves (dark bands) are obtained by setting $\Delta s = m\lambda$ in (3), where λ is the wavelength of the light used. For small birefringence $\delta = \epsilon - \omega$, an expansion of (4) to lowest order in δ gives

$$\frac{\lambda\omega^2}{t\delta}m = \frac{\sin^2\theta(m)}{\sqrt{1-\dfrac{\sin^2\theta(m)}{\omega^2}}} \tag{5}$$

[1] There is a typographical error in Kamb (1970), eqn. (8): the quantities n_1 and n_2 in this equation should read n_1^2 and n_2^2. Earlier references to the basic path-difference equation (4) of Kamb (1970) are Neumann (1834) and Pockels (1906), kindly supplied by D. J. Fisher.

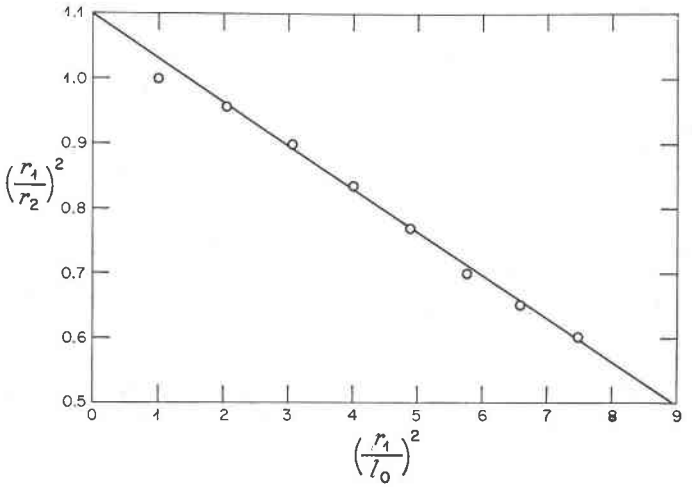

FIG. 3. Plot of $[r_1(m)/r_2(m)]^2$ against $[r_1(m)/l_0]^2$ for successive orders m of isochromes in centered uniaxial figures of types 1 and 2. The points represent the measurements of Fisher (1960), given in columns 2 and 5 of Table 1. The straight line is fitted by eye.

(5) can be solved for $\sin^2\theta$:

$$\sin^2\theta(m) = ms_1\left(\sqrt{1+\frac{1}{4}\frac{s_1^2m^2}{\omega^4}}-\frac{1}{2}\frac{s_1m}{\omega^2}\right) \tag{6}$$

where $s_1=\lambda\omega^2/t\delta\cong\sin\theta(1)$. For small m, the factor in parenthesis on the right side of (6) remains constant. r_1, which is proportional to $\sin\theta$ from (1), then goes as $\sqrt{m}$. To this approximation we expect the "$\sqrt{m}$ rule" quoted by Fisher (1960) to hold.

Because of uncertainty in the exact applicability of Mallard's Rule, it is best to evaluate the constant s_1 in (6) by using the $r_2(m)$ data in Table 1. To do this, $\theta(m)$ values were obtained from the data using equation (2), and s_1 was adjusted to give the best fit to $\theta(m)$ values calculated from (6). The result is $s_1=\lambda\omega^2/r\delta=0.0637$, corresponding to $\theta(1)=14.6°$. If for the muscovite sample used, $\delta=0.033$ and $\omega=1.585$ (values obtained from ordinary, biaxial muscovite by averaging the β and γ indices), then the s_1 value requires $t=0.52$ mm, a reasonable inferred thickness for the muscovite plate. ($\lambda=435.9$ $m\mu$ for Hg vapor.)

With the constants s_1, l_1, and l_2 so determined, we can calculate from equations (6), (1), and (2) the radii $r_1(m)$ and $r_2(m)$ expected in Fisher's experiments. They are given in columns 3 and 6 of Table 1. The agreement between calculated and observed radii is good, even for most of the

curves of higher order, for which Fisher suggested some uncertainty in the measured values.

The comparison between the $r_1(m)$ values measured by Fisher and calculated on the basis of equation (1) provides a direct test, for Fisher's objective, of the validity of Mallard's rule, expressed in (1). The agreement is good, although perhaps slightly poorer at the largest orders ($m=7-9$). These results test Mallard's law up to an effective numerical aperture $\sin\theta(9)=0.72$, hence over a large portion of the $N.A.$ 0.85 of conventional objectives used in conoscopic work. (The objective used by Fisher was a special one of high $N.A.=1.45$.)

Note that the radii $r(m)$ calculated simply from the "$\sqrt{m}$ rule" (Table 1, column 4) show significant departures from the measured radii $r_1(m)$ for the larger orders. This shows that the second factor on the right side of (6) has an appreciable effect on the measurements.

The reduced size of the r_1 radii, by comparison with the corresponding r_2 radii in Table 1, espresses quantitatively the relative "compression" of the outer part of the type-1 interference figure, which was noticed by Fisher (1960, Fig. 3 and p. 18). From the forgoing discussion it is seen that this effect is directly traceable to the difference between the $\sin\theta$ and $\tan\theta$ "projection factors" of equations (1) and (2). In effect, the type-1 figure is projected orthographically, the type-2 figures gnomonically.

I wish to thank D. J. Fisher for calling my attention to the measurements that provide the basis for this note.

References

Fisher, D. J. (1960) *Indian Mineral.* **1**, 11.

Kamb, B. (1970) Interference colors in flash figures. *Amer. Mineral.* **55**, 767.

Neumann, F. (1834) *Pogg. Ann.* **33**, 265.

Pockels, F. (1906) *Lehrbuch der Kristalloptik.* Teubner, Berlin, p. 231, eqn. (2).

Manuscript received, August 7, 1970; accepted for publication, September 71, 1970.